A weather radar data processing module for storm analysis

Ioannis N. Daliakopoulos and Ioannis K. Tsanis

ABSTRACT

A pre- and post-processing weather radar data module was developed in the Matlab suite of software with GIS data exchange abilities for storm event analysis. During pre-processing, each radar sweep is converted from spherical to Cartesian coordinates in the desired temporal and spatial resolution. The module's functionality in post processing includes radar data display, geo-referencing over GIS maps, data filtering with the Wiener filter and single or multiple sweep processing. The user can perform individual storm cell detection and tracking, resulting in the storm's average velocity and track length. The tested methods are modifications of the LoG (Laplacian of the Gaussian) blob detection method and a Brownian particle trajectory linking algorithm. Radar reflectivity factor (Z) data can be referenced over predefined rainfall (R) gauges in order to determine the radar Z–R equation parameters. The user can also produce spatially distributed precipitation estimates by using standard Z–R equations from the literature. The module's functionality is demonstrated using data from a rainfall event captured by the NSA Souda Bay C-Band radar during a storm in October 2006. Results show that the Rosenfeld Tropical Z–R equation is the one that gives a satisfactory description of the spatial and temporal precipitation distribution of the investigated event.

Key words | detection, filters, Matlab, precipitation, radar, tracking

Ioannis N. Daliakopoulos
Ioannis K. Tsanis (corresponding author)
Department of Environmental Engineering,
Technical University of Crete,
Chania 73100,
Greece
E-mail: *tsanis@hydromech.gr*

INTRODUCTION

Precipitation intensity can be estimated using ground precipitation gauges or a combination of gauges and radar data. Even though measurement errors such as undercatch (Adam & Lettenmaier 2003; Daliakopoulos *et al.* 2006) do exist, the precision of precipitation gauges is generally adequate and the derived ground level precipitation product is reliable. Nevertheless, coverage is often limited by topography and cost (Borga *et al.* 2000). Other effects such as the gradient of precipitation with altitude (Naoum & Tsanis 2004) can cause conventional interpolation of the precipitation variable to inadequately represent reality. Therefore, precipitation data can be insufficient for use with a distributed hydrological model. Weather radars have thus become an invaluable tool for the nowcasting of precipitation, that, besides their limitations (Delrieu *et al.* 2009), provide detailed spatial and temporal information (Divjak *et al.* 1999). Figure 1 shows the basic operation principles of weather radars from target detection to data recording and display using plan position indicator (PPI).

To make full use of the inherent radar capabilities, it is necessary to know the main sources of radar errors and limitations in order to properly interpret the data. Radar-rainfall error sources have been recognized and discussed in the literature for more than three decades (Harrold *et al.* 1974; Wilson & Brandes 1979; Zawadzki 1984; Austin 1987; Joss & Waldvogel 1990; Kitchen & Jackson 1993; Joss & Lee 1995). Michelson *et al.* (2005) present a comprehensive list of error sources that can be related to various factors from environmental conditions to radar hardware and model uncertainty. Several types of data corrections can be applied by the radar signal processor. For example, the R^2 correction normalizes the reflectivity with respect to distance from the radar transmitter, the signal degeneration correction calculates the degeneration due to atmospheric gases

doi: 10.2166/hydro.2011.118

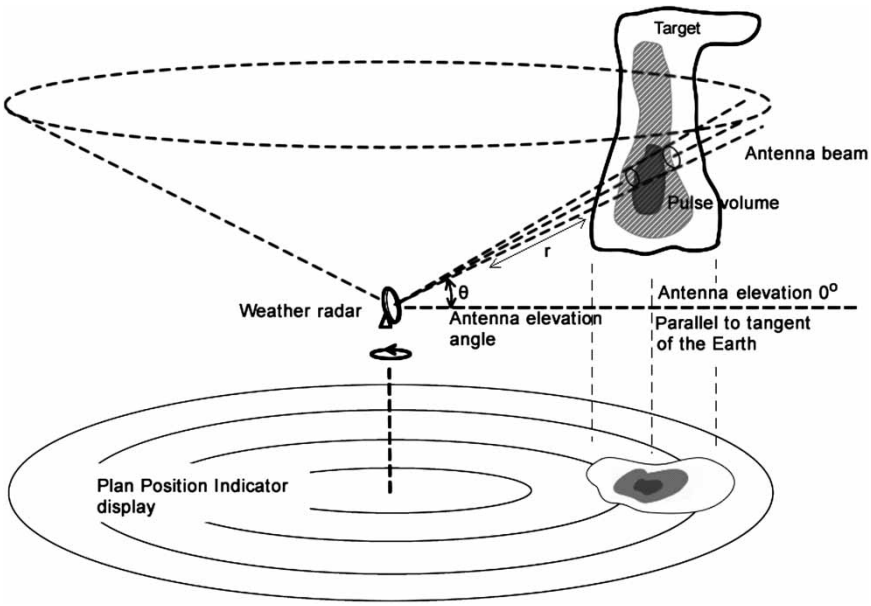

Figure 1 | Weather radar operation principles producing a plan position indicator (PPI) display.

and clutter filtering represses the signal under a given threshold accounting for undesirable objects. The corrected information can contain some or all of the possible corrections but even after the corrections are made, various artefacts can still appear in radar data fields in several forms of noise (Divjak *et al.* 1999).

Noise introduces sharp gradients in otherwise smooth weather fields and can be eliminated, to some extent, by suitable texture smoothing. However, the smoothing process affects weather data, resulting in a loss of fine-scale details (Divjak *et al.* 1999). When noise is largely caused by a number of small sources, the system and observation noise can be regarded as a white Gaussian distribution (Maybeck 1979). A commonly used method of noise suppression in weather radar data is that of thresholding (Sugier *et al.* 2002; Chumchean *et al.* 2008). Nicol *et al.* (2004) used a threshold on neighboring maximum local gradients to account for ground clutter generated noise whereas Seminario *et al.* (2001) used spectral analysis to filter noise in a polarimetric radar product. In more recent work, Villarini *et al.* (2008) compared a non-parametric framework based on the approach of Ciach (2003) with a parametric framework.

Over the past 40 years many algorithms have been developed for storm tracking (Johnson *et al.* 1998). Commonly, spatial cross correlation is used to determine the movement of storms (Bellon & Austin 1984; Austin 1987; Einfalt *et al.* 1990; Fabry *et al.* 1994; Tsanis *et al.* 2002). When applied to larger fields of reflectivity, this algorithm can provide accurate speed and direction information. According to a more recent technique, centroid identification and tracking can capture individual, isolated storms more effectively (Jackson 1993). Wilk & Gray (1970) applied this algorithm to data from the WSR-57 radar for the estimation of storm motion and precipitation. This technique and variations were applied by Zittel (1976), Brady *et al.* (1978), Crane (1979), Rosenfeld (1987) and Blanchet *et al.* (1991).

Mecklenburg *et al.* (2002), among others, present a comprehensive list of quantitative precipitation forecast (QPF) methods and tools. According to various sources, radar data manipulation software includes, but is not limited to the following.

1. EDGE (EEC 2011) is a state-of-the-art commercial license software developed by the Enterprise Electronics Corporation (EEC) and designed to work only with EEC's radar output. This software supports a large number of data displays and corrections etc. but there is no export capability with GIS software.
2. The GFS forecasting algorithm, described by Toussaint *et al.* (2000a), uses cloud cell tracking or TREC/

COTREC motion field tracking in order to compute motion vector over a series of radar images.

3. DUR-TOOLKIT, described in Toussaint *et al.* (2000b), deals with visualization, pre- and post-processing and filtering. It is developed in C++ and therefore has to be portable; nevertheless there is no information about storm tracking or GIS interoperability.
4. Abacus, (Athanasiadis *et al*. 2009) has been developed as a radar data management and decision support system covering visualization, statistical estimations and weather conditions assessments. It is mainly a management platform for warnings etc.

The objective of the current paper is to develop a module that can serve as a workbench for scientific testing, experimenting and visualization allowing for easy integration of innovative functionalities for weather radar data processing. These functionalities include data preprocessing, filtering and visualization as well as storm detection and tracking. New algorithms on noise filtering, storm cell detection and tracking can be easily added to the module. Finally, the module allows for data export to GIS for further processing and visualization.

METHODOLOGY

The weather radar records the data in the form of *volumes*. A volume is constituted from a set of sweeps which in turn are made up from a set of beams (rays). Each beam consists of a number of *range gates* which represents the sampling resolution along the length of each beam. Each gate is the integration of the radar pulse for a particular distance that depends on the system configuration. The complete beam range covered by the radar is the product of the number of gates and the length of each gate.

As with most environment data, graphical display is an indispensible tool when seeking patterns, generating hypotheses and assessing the fit of proposed models (Tsanis & Gad 2001). The PPI (Figure 1) is the most common type of radar display. As the radar antenna rotates, a radial trace sweeps around it so the distance from it and the height above ground can be drawn as concentric circles. A simple data display such as this is often insufficient as a high degree of uncertainty affects precipitation estimates based on radar measurements (Anagnostou *et al*. 1999). Alternative displays include the constant altitude plan position indicator which gives a horizontal cross-section of data at constant altitude, vertical composite which produces images of the maximum reflectivity in a layer above ground, and others, according to the need of the users.

Pre-processing

The radar data are originally stored in polar coordinates and have to be converted to Cartesian coordinates in order to be displayed and processed. Along a single beam, the radar records measurements based on radar elevation angle θ_s and slant range r. The distance s covered by the beam along the earth's surface is given by (Doviak & Zrnić 1993):

$$s = k_s a \sin^{-1}\left(\frac{r\cos\theta_s}{k_s a + h}\right) \quad (1)$$

where h is the height of the center of the radar beam given by:

$$h = [r^2 + (k_s a)^2 + 2rk_s \sin\theta_s]^{1/2} - k_s a \quad (2)$$

In both equations, a is the earth's radius and k_s is a multiplier which depends on atmospheric conditions. Assuming standard atmosphere, k_s is equal to 4/3 (Doviak & Zrnić 1993). More complex equations like the ones presented by Gao *et al*. (2006) take into account the influence of thermographic profiles along the path of the radar beam.

For a complete sweep of the horizon at a single radar elevation θ_s, data are represented by a set of polar coordinates (s, θ_r). The corresponding Cartesian x, y coordinates can be estimated using:

$$x = s\cos(\theta_r) \quad (3)$$

$$y = s\sin(\theta_r) \quad (4)$$

This process produces a scatter of (x, y) pairs. In order to store and display this data in an efficient way compatible

with most GIS applications, the data can be converted to an equally spaced grid form. At useful resolutions, that is, over 500×500 m, the disk storage required for a rasterized radar image is several orders of magnitude smaller than the raw radar data product and the produced file can be easier to handle and process. Unfortunately, rasterizing normally involves interpolating the data to a grid with fixed cell size which inherently degrades the original information. The extent of the grid used to interpolate data was chosen to be the horizontal projection of the maximum radius in the lower sweep of each volume. Finding a reliable interpolation scheme, especially for unevenly distributed data, represents a great challenge with the derived data seldom conveying additional information. In the case of weather radars, missing data signifies the absence of atmospheric phenomena and therefore estimating interpolated values at all costs can be meaningless, as suggested by Djurcilov & Pang (1999). Here, instead of a computationally expensive method like kriging (Simpson *et al.* 1998; Djurcilov & Pang 1999), the nearest neighbor (Goovaerts 1997) interpolation technique is used.

Noise removal – the Wiener filter

After interpolation, radar data images may contain noise. A digital signal s can deteriorate due to noise n with the resulting signal $\hat{s}$ often modeled as a simple summation $\hat{s} = s + n$. This noise can appear in several forms. In salt and pepper or speckle noise a small number of image pixels show a great discrepancy in color and intensity from their neighbors as a result of random fluctuations in the return signal from objects that are smaller than the radar image-processing resolution (Simonett 1970). The term salt and pepper originates from the black and white pixels that corrupt the image when viewed in monochrome. Gaussian noise, on the other hand, usually causes small changes in the original pixel values with the amount of distortion versus the occurrence frequency being normally distributed. Gaussian distribution is adopted assuming a sufficiently large number of pixels and noise for each pixel as an independent random variable.

Methods of de-noising radar fields could include convolving the original data with a low-pass or smoothing filter. De-noising s without a prior knowledge of its components requires making assumptions of the noise and signal characteristics. In general, radar measurement errors are not Gaussian (Krajewski & Ciach 2004). For a linear approach known as the Wiener filter (Wiener 1949), the procedure involves designing a filter $h[x]$ such that:

$$s[x] = h[x]\,\hat{s}[x] = h[x](s[x] + n[x]) \tag{5}$$

so that when the filter is convolved with the corrupted signal, the original signal can be recovered. Then, this constraint is transferred in the frequency domain and a quadratic error functional E is constructed:

$$E(H(\omega)) = \int d\omega [H(\omega)(S(\omega) + N(\omega)) - S(\omega)]^2 \tag{6}$$

where ω is the frequency parameter and capital symbols are used to denote the filter, the signal and the noise in the frequency domain, respectively. In order to simplify this expression the signal and noise are assumed to be statistically independent. To minimize, we differentiate and set equal to zero:

$$H(\omega) = \frac{S^2(\omega)}{S^2(\omega) + N^2(\omega)} \tag{7}$$

The process is described in detail by Farid (2008). Intuitively, this frequency response makes sense as when the signal is significantly stronger than the noise the response is close to 1, that is, the frequencies are passed. On the other hand, when the signal is significantly weaker than the noise the response is close to 0, that is, the frequencies are stopped. Assumptions about the statistical nature of the signal and noise are also necessary. For example a common choice is to assume white noise, $N(\omega)$ is constant for all ω, and, for natural images, to assume that $S(\omega) = 1/\omega^p$. Unfortunately denoising has the expected side effect of losing some of the image sharpness, as the Wiener filter is a low-pass filter.

In Matlab, the *wiener2* function is an adaptive application of the Wiener filter that estimates the local mean and variance around each pixel after Lim (1990):

$$\mu = \frac{1}{NM} \sum_{n_1 n_2 \in \eta} \alpha(n_1, n_2) \tag{8}$$

$$\sigma^2 = \frac{1}{NM}\sum_{n_1 n_2 \in \eta} \alpha^2(n_1, n_2) - \mu^2 \quad (9)$$

where n is the N-by-M local neighborhood of each pixel in the image. Then *wiener2* creates a pixel-wise Wiener filter using these estimates:

$$b(n_1, n_2) = \mu + \frac{\sigma^2 - v^2}{\sigma^2(\alpha(n_1, n_2) - \mu)} \quad (10)$$

where v^2 is the noise variance. If the noise variance is not given, *wiener2* uses the average of all the local estimated variances. Figure 2 shows the effect of a 3×3 Wiener filter on radar data.

Besides conventional image filters, more complex techniques such as neural networks (Teschl *et al.* 2007) and support vector machine (Ziyang *et al.* 2008) have been used to de-noise radar data, but are beyond the scope of the current paper.

Z–R conversion

The quantity that is measured by the radar is reflected energy called reflectivity which depends upon the size, shape, aspect, and dielectric properties of targets in atmosphere. *Reflectivity Factor Z* is measured in mm^6/m^3 and is a function of the number and size of drops within a given volume. The values of the reflectivity factor cover a wide range so they are commonly expressed in units of dbZ. The radar rainfall rate can be obtained by using an empirical *Z–R* relation either from literature or deduced from measurements of drop-size distributions in natural rain (Battan 1973). The *Z–R* relation has the form:

$$Z = aR^b \quad (11)$$

where a and b are empirical coefficients that depend on the type of precipitation (snow, rain, convective or stratiform) and geographic location (Austin 1987).

As the meteorological radar does not measure precipitation directly, error sources can influence the accuracy and precision of the estimates (Zawadzki 1984). The *Z–R* relation is non-linear and can vary depending on the geographic region and the event of rainfall to be estimated, which makes the correct choice of parameters complex (Battan 1973). The differences in radar estimates and terrain rain gauge measurements can in certain cases reach 100% (Wilson & Brandes 1979) or larger. The sensitivity analysis

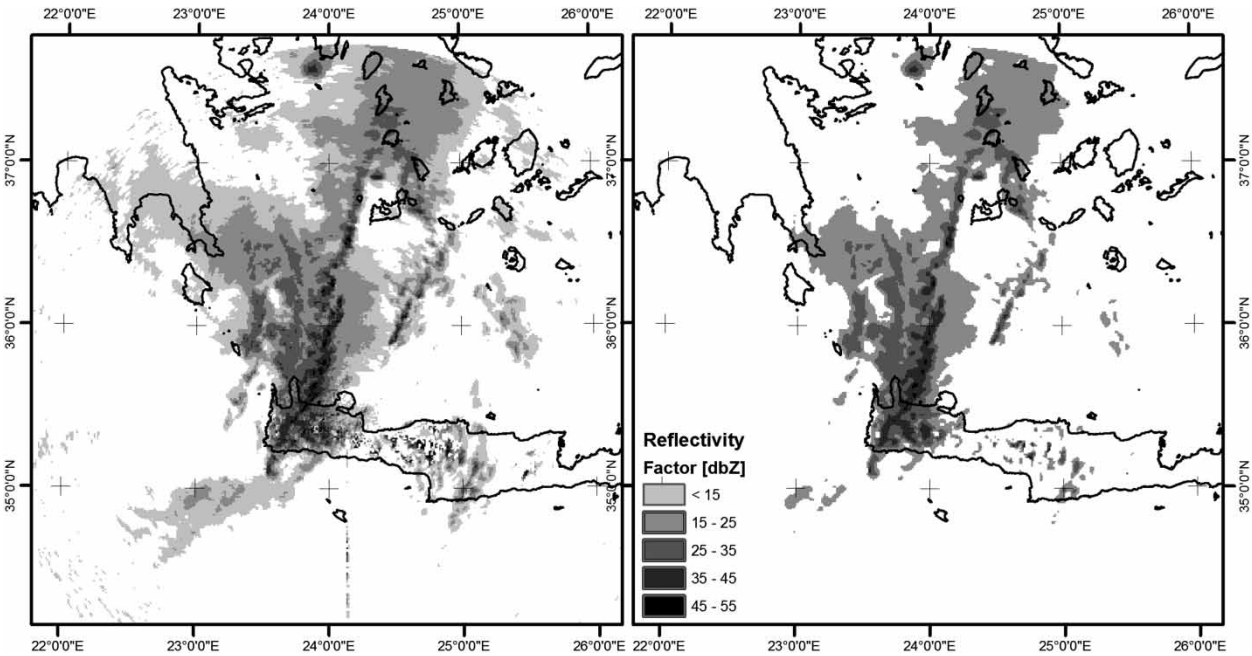

Figure 2 | Wiener filter application on radar data. Raw reflectivity factor data (left) is processed with a 3×3 pixels Wiener filter and a 15 dbZ cut-off filter (right).

of precipitation estimates from the radar data of OSF (operational support facility) and the 'WSR-88D Adaptive Parameter Working Group' showed that the choice of valid Z–R relation can provide the most important improvement in the precipitation estimates (Belville 1999). This shows the importance of calibrating a suitable Z–R relation for the calculation of rainfall.

Storm cell detection

Techniques involving pattern recognition and image processing (e.g. Blackmer *et al.* 1973; Einfalt *et al.* 1990) have successfully been supplied to describe and recognize storm cells. Here, a method known as blob detection is being used in order to detect the storm cell centers. One of the first and most common blob detection techniques is based on the Laplacian of the Gaussian (Lindeberg 1998). A given image $f(x,y)$ can be convolved by a Gaussian kernel h_g of width σ^2:

$$h_g(x,y,\sigma) = \frac{1}{2\pi\sigma^2} e^{-(x^2+y^2)/2\sigma^2} \tag{12}$$

to give a representation:

$$L(x,y,\sigma) = h_g(x,y,\sigma) \cdot f(x,y) \tag{13}$$

Then, the Laplacian operator is computed as:

$$\nabla^2 L = L_{xx} + L_{yy} \tag{14}$$

which usually results in strong positive responses of coherent reflective maxima of extent σ (Wildenauer *et al.* 2007). Essentially, the image $f(x,y)$ is processed with a filter given by:

$$h(x,y,\sigma) = \frac{(x^2+y^2-2\sigma^2)h_g(x,y,\sigma)}{2\pi\sigma^6 \sum_x \sum_y h_g(x,y,\sigma)} \tag{15}$$

The characteristics of the Gaussian kernel can be used as search criteria for the storm cells of different diameter and intensity.

Storm cell tracking

Having located dominant storm cell centers in a sequence of radar products, cell locations are matched up with corresponding locations in later frames to produce the trajectories in $\rho(r,t)$. This requires determining which storm cell in a given frame is the most likely to match the one appearing in the adjacent frame. Tracking more than one storm cell requires defining the most probable set of N identifications between N locations in two consecutive frames. If the cells are indistinguishable, as for most storm cells, this likelihood can be estimated only by proximity in the two images. The corresponding algorithm for trajectory linking can be initiated by considering the dynamics of non-interacting Brownian particles as described in detail by Crocker & Grier (1996). For a given storm cell moving on a plane, the probability that it travels a distance δ in time τ is:

$$P(\delta|\tau) = \frac{1}{4\pi D\tau} \exp\left(-\frac{\delta^2}{4D\tau}\right) \tag{16}$$

where D is the diffusivity coefficient. Respectively, for N non-interacting identical particles the probability distribution can be derived:

$$P(\{\delta_i\}|\tau) = \left(\frac{1}{4\pi D\tau}\right)^N \exp\left(-\sum_{i=1}^{N} \frac{\delta_i^2}{4D\tau}\right) \tag{17}$$

The most likely storm cell trajectory from one frame to the next is the one which maximizes $P(\{\delta_i\}|\tau)$ or, equivalently, minimizes $\sum_{i=1}^{N} \delta_i^2$. This criterion has been shown to perform well even for interacting cells provided a sufficiently small time interval between frames (Crocker & Grier 1996). Figure 3 shows an example of storm cell detection (nodes) and tracking (solid arrows). In order to account for storm cells that are not detected in all frames, their last known location is stored and matched with unassigned cells that appear in subsequent frames and fit the distance criterion.

Detection and tracking methodologies with similar algorithms, like CELLTRACK and COTREC are described by Kyznarová & Novák (2009).

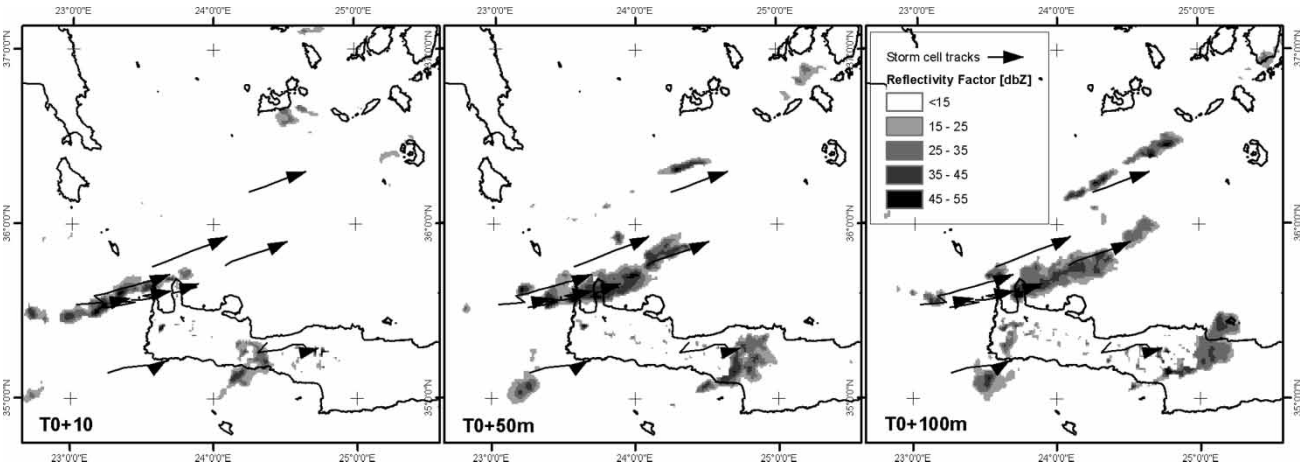

Figure 3 | Storm cell center detection and tracking during a 100 m interval consisting of 10 radar scans (only three shown).

MODULE STRUCTURE

An outline of the structure of the module is presented in Figure 4. The raw radar data are inputted to the module which initially converts them to a native format for subsequent read/write access. The module is comprised of a total of five interfaces that allow the user to manipulate the data and produce output.

The only currently available display mode is the PPI (Figure 1), which is the most common type of radar data display. The transmitting radar is usually placed in the center of the display so equal distances from it can be drawn in concentric circles. As the radar is revolving, the PPI trace appears to scan concentrically from the center to the largest distance of emission. North is found at the top of the display while the signal depicts the reflectivity at a single radar elevation. Therefore, it is possible to have one PPI display for each elevation scan.

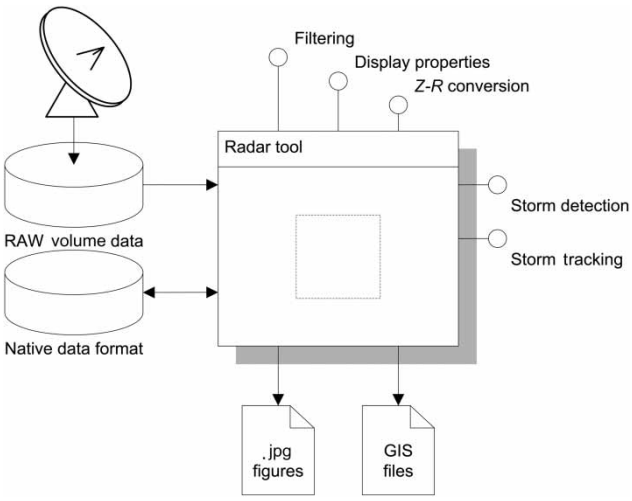

Figure 4 | Weather radar data module features.

The *Filter selection* menu gives the user the ability to choose among available preprocessing options for a selected object. Filters are modular so more options can be added in future versions. The currently available options are a 15 db threshold, an application of the noise reduction Wiener filter, a combination of the above and no filtering at all.

Depending on the season, geographic location, and expected weather type some standard *Z–R* relationships can be used to translate reflectivity into precipitation rate. Table 1 lists the *Z–R* relationships currently available along with the WSR-88D OSF recommendations for selecting the best *Z–R* relationship for most types of precipitation events (Belville 1999).

When mixed precipitation types are present the WSR-88D OSF suggests that sites should select a *Z–R* relationship based on the dominant type of precipitation. The use of a unique *Z–R* equation for all reflectivity observations regardless of differences in rainfall drop size distributions and atmospheric conditions can result in misinterpretation of the data (Atlas *et al.* 1999). Optionally,

Table 1 | Typical *Z–R* relationships including the phenomena for which their use is recommended in literature

Relationship	Optimum for	Also recommended for
Marshall–Palmer ($Z = 200R^{1.6}$)	General stratiform precipitation	
East-Cool Stratiform ($Z = 130R^{2.0}$)	Winter stratiform precipitation – east of continental divide	Orographic rain – East
West-Cool Stratiform ($Z = 75R^{2.0}$)	Winter stratiform precipitation – west of continental divide	Orographic rain – West
WSR-88D Convective ($Z = 300R^{1.4}$)	Summer deep convection	Other non-tropical convection
Rosenfeld Tropical ($Z = 250R^{1.2}$)	Tropical convective systems	

the *Z–R* relationship can be calibrated using data from gauges located within the radar's range.

The *Storm cell detection* function allows the user to change blob detection parameters in order to enhance the process. Parameters adjust the minimum diameter and the minimum local maximum intensity of the detected cells, resulting in alternative storm dynamics representations. Finally, the *Storm cell tracking* function allows the user to change tracking parameters in order to enhance the process. Parameters adjust the maximum distance between two storm cell instances in two consecutive radar scans.

The above operations are divided in two main layers that deal with: (a) operations of single radar scans, and (b) batch operations. The output can be either shown on the screen or saved in various formats such as common raster files (.bmp, .jpg, etc.) or geo-referenced raster files as Geotiff (Burrows 2000) and arcgrid (ESRI 1992). Geotiff and arcgrid formats can be handled by ESRI applications such as ArcMap, making display along with other geo-referenced layers as well as spatial calculations an easy procedure. Additionally, some objects like storm cell centers and storm tracks can be exported in the form of shape files which are also compatible with a wide range of GIS applications.

CASE STUDY

The module's functionality is demonstrated using data from one rainfall event that was captured by the NSA Souda Bay C-Band radar during an October 2006 storm. The Radar of Souda Bay Naval Base is a model SWR-250C C-Band Radar constructed by EEC (Enterprise Electronics Corporation). The acquired data are further processed by the computer workstation software to generate and display a variety of weather products. The radar has been set up to perform five sweeps with elevations from 0.5 to 14°. The radar radiates a beam every 0.95° of rotation thus producing 378 rays of data for each of the five sweeps. With 239 gates per beam and a gate length of 1,000 m the maximum range of the radar is 239 km. Due to effects such as overshooting associated with the transmitter elevation, partial beam filling that can cause reflectivity factor and precipitation rate underestimation (e.g. Joss & Waldvogel 1990; Durden *et al.* 1998) and beam attenuation (e.g. Paulitsch *et al.* 2009; Cremonini & Bechini 2010), quantitative precipitation estimation at ranges beyond 100 km is problematic (Uijlenhoet *et al.* 2006).

In October 2006, a frontal depression moved eastward towards the central Mediterranean and crossed the island of Crete at midday on October 17. This depression caused a high-intensity short-duration heavy rainfall resulting in a flash flood event in the Almyrida basin, a 25 km^2 watershed located in the northwest part of the island. At the time of the event the neighboring rain gauge of Souda Bay (16 km) recorded a maximum hourly precipitation of 25.2 mm and a daily gauge located just 3 km from the watershed recorded 220 mm. Similar to other intense precipitation events in the Mediterranean (Berne *et al.* 2009), the flash flood was devastating, leading to the loss of one life and over €1M in damages in Almyrida alone, and leaving a total damage toll of approximately €3M. With the help of radar data it was possible to reconstruct the event and identify characteristics of the storm such as storm cell velocity and precipitation intensity. The developed module can process radar data and export them to GIS for a better visualization and understanding of the meteorology of the event. This is more efficient than building the code within a GIS system which is slow and not as versatile (Naoum & Tsanis 2003).

On the day of the event, raw radar data were acquired at 15-min intervals except for several missing scenes due to power outages in the area. Figure 5 shows the reflectivity recorded shortly after the formation has crossed over the island passing through two mountaintops with a northward direction. Data were interpolated to a 500 m × 500 m Cartesian grid providing adequate resolution for further processing. The observations were filtered using a Wiener filter coupled with a 15 db threshold to remove noise and insignificant reflectivity values. Then, it became clear that

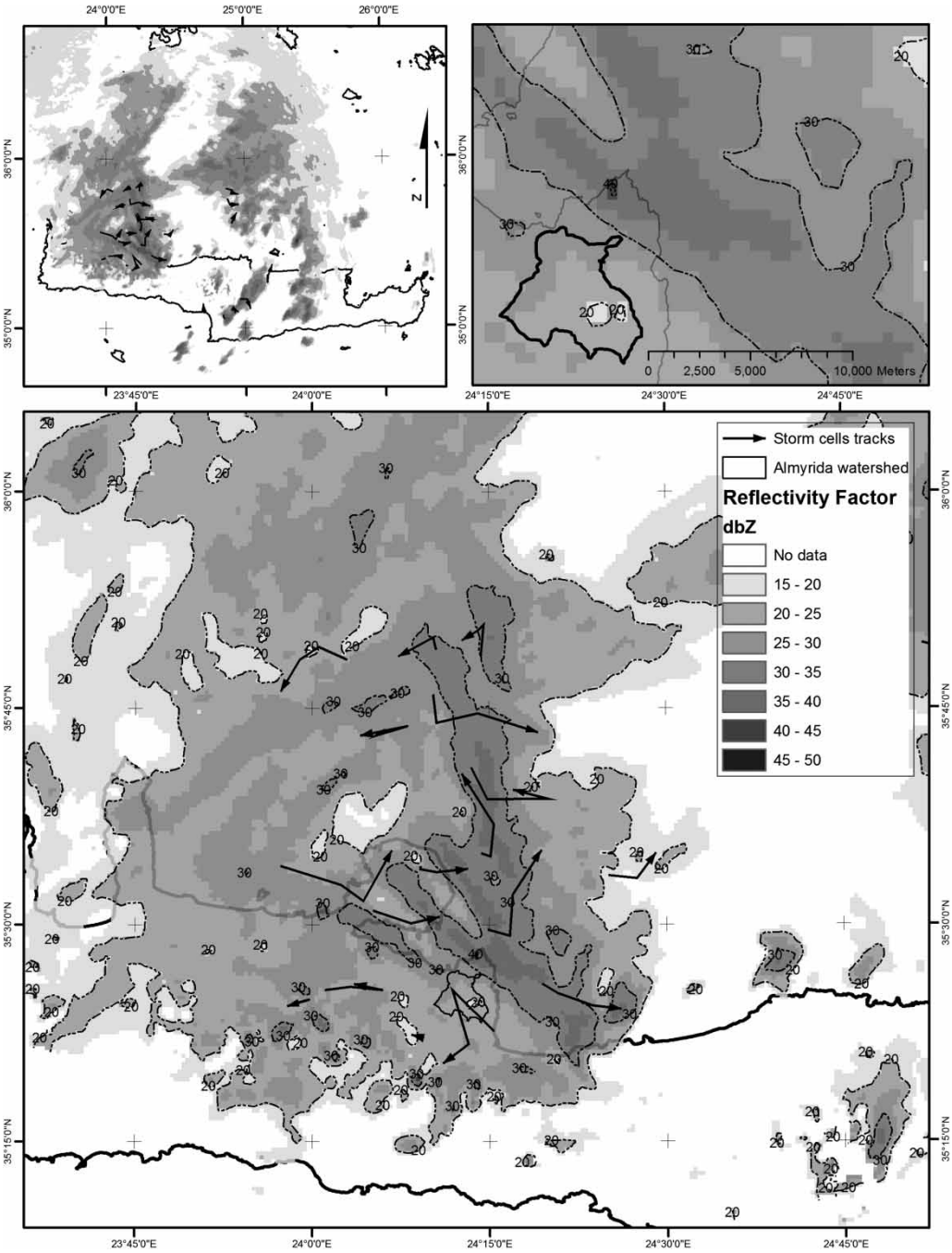

Figure 5 | Reflectivity of the storm that hit the north coast of Crete on October 17, 2006 as it was recorded on 15:13 UTC. Arrows show the direction of individual storm cells from 15:13 to 15:58 UTC.

Table 2 | Rainfall rate comparison (values in mm/h). The maximum reflectivity factor recorded over Almyrida at 15:13 UTC of October 17, 2006 is included for reference

dbZ	Marshall–Palmer	East-Cool Stratiform	West-Cool Stratiform	WSR-88D Convective	Rosenfeld Tropical
15.00	0.32	0.49	0.65	0.20	0.18
25.00	1.33	1.56	2.05	1.04	1.22
35.00	5.62	4.93	6.49	5.38	8.29
40.33	12.09	9.11	11.99	12.92	23.04
45.00	23.68	15.60	20.53	27.86	56.46
55.00	99.85	49.32	64.93	144.28	384.64

the system was essentially a large cyclone with a maximum diameter of about 200 km. Storm cell detection and tracking produced vectors that were exported to GIS along with reflectivity values. Vectors depicted individual storm cell movement within the formation during the hours of the storm, showing the cyclone's center persisting to the north-east of Almyrida, a position that favors orographic uplift from the mountain volumes in the south of the watershed.

Table 2 shows rainfall rates versus dbZ for all cited models. For reference, the maximum reflectivity factor recoded over Almyrida (40.33 dbZ) is also shown. The Rosenfeld Tropical conversion (Figure 6) which estimates a maximum precipitation rate of 23 mm/h is in good agreement with the field data. This rate is estimated offshore from Almyrida and can be tracked back over the watershed during the time of the flood. Other models estimate lower rainfall rates giving a less representative image of the rain fields for this particular storm. At the time of the study, the validation or calibration of a custom *Z–R* relationship was not possible as available terrain gauge data have inadequate temporal and spatial resolution. Nevertheless, the results showed the spatial and temporal distribution of the formation that caused the flash flood which by itself proved the usefulness of this module in the study of extreme events via analysis of weather precipitation radar data.

CONCLUSION

A new module for weather radar data pre- and post-processing was developed in Matlab. This paper briefly presents its functionalities with respect to data analysis and visualization. The tool allows for modularity, therefore serving as a workbench for the comparison of different algorithms. Each of the operations performed (i.e. filtering, storm cell detection, etc.), can be executed using alternative

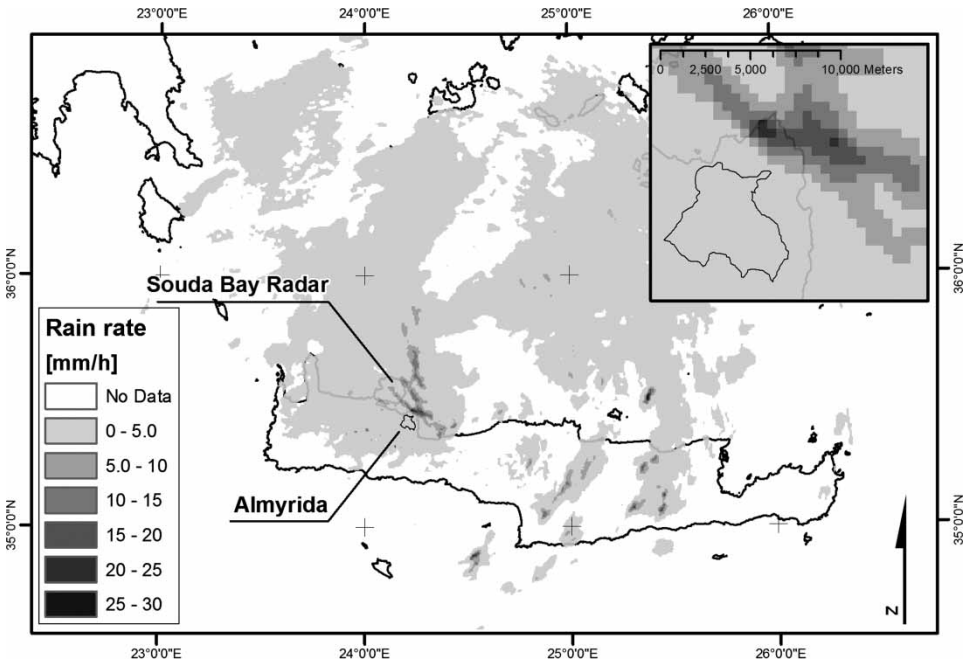

Figure 6 | *Z–R* translation of a reflectivity scan recorded on 15:13 UTC on October 17, 2006 using the Rosenfeld Tropical equation.

algorithms. Each new algorithm can be added as part of the module GUI in a new option of the corresponding drop down menu. This allows for quick testing and identification of the most appropriate methodology for each case. Results can be compared visually and mathematical computations can be performed in any arcgrid-compatible environment.

Regarding the default algorithms, each has its own advantages and limitations. For example, the storm cell tracking algorithm performs best with distinguishable storm cells having consistent paths. Irregular or rapid storm cell motion and ambiguous formations that merge and divide hinder the effectiveness of the algorithm. Nevertheless, using the algorithms in a modular environment allows for quick and efficient testing and result comparison for algorithm improvement and extension.

The module was tested in the study of a flash flood event in north-western Crete in an attempt to reconstruct the meteorological conditions that lead to its outbreak. The functionalities of data preprocessing, filtering and storm cell detection and tracking gave a good representation of the storm formation and movement. Particularly, the Rosenfeld Tropical Z–R equation provided an adequate fit with precipitation rate measurements during the event. Finally, the results were exported in a GIS-compatible format allowed for better visualization and easier manipulation in a friendly environment.

ACKNOWLEDGEMENTS

The research presented in this paper has been carried out as part of the European Commission FP6 funded project, HYDRATE. The authors also wish to thank Enterprise Electronics Corporation (EEC) for providing data and support throughout this research.

REFERENCES

Adam, J. C. & Lettenmaier, D. P. 2003 Adjustment of global gridded precipitation for systematic bias. *J. Geophys. Res.* **108** (D9), 4257.

Anagnostou, E. N., Krajewski, W. F. & Smith, J. 1999 Uncertainty quantification of mean-areal radar-rainfall estimates. *J. Atmos. Oceanic Technol.* **16**, 206–215.

Athanasiadis, I. N., Milis, M., Mitkas, P. A. & Michaelides, S. C. 2009 A multi-agent system for meteorological radar data management and decision support. *Environ. Modell. & Softw.* **24**, 1264–1273.

Atlas, D., Ulbrich, C. W., Mark Jr., F. D., Amitai, E. & Williams, C. R. 1999 Systematic variation of drop size and previous termradarnext term-rainfall relation. *J. Geophys. Res.* **104**, 155–169.

Austin, P. M. 1987 Relation between measured radar reflectivity and surface rainfall. *Mon. Weather Rev.* **115**, 1053–1070.

Battan, L. J. 1973 *Radar Observation of the Atmosphere*. The University of Chicago Press, Chicago.

Bellon, A. & Austin, G. L. 1984 The accuracy of short-term radar rainfall forecast. *J. Hydrol.* **70**, 35–49.

Belville, J. D. 1999 Recommended parameter changes to improve WSR-88D rainfall estimates during cool season stratiform rain events. MEMORANDUM FOR: NWFO WSR-88D Operations POCs. Available from: http://www.roc.noaa.gov/ops/z2r_osf5.asp (accessed 14 December 1999).

Berne, A., Delrieu, G. & Boudevillain, B. 2009 Variability of the spatial structure of intense Mediterranean precipitation. *Adv. Water Resour.* **32** (7), 1031–1042.

Blackmer, R. H., Duda, R. O. & Reboh, E. 1973 Application of pattern recognition techniques to digitized weather radar data. Stanford Research Institute, Menlo Park, CA, Rep. 36072.

Blanchet, B., Neuman, A., Jacquet, G. & Andrieu, H. 1991 Improvement of rainfall measurements due to accurate synchronization of rain gauges and due to advection use in calibration. In: *Hydrological Applications of Weather Radar* (I. D. Cluckie & C. G. Collier, eds.). Ellis Horwood, Chichester, pp. 213–218.

Borga, M., Da Ros, D., Fattorelli, S. & Vizzaccaro, A. 2000 Influence of various weather radar correction procedures on mean areal rainfall estimation and rainfall-runoff simulation. In *Proc., 3rd International Symposium on Hydrologic Applications of Weather Radar*, ABRH.

Brady, P. J., Schroeder, M. J. & Poellot, M. R. 1978 Automatic identification and tracking of radar echoes in HIPLEX. In *Preprints, 18th Conf. on Radar Meteorology*, Atlanta, GA, pp. 139–143.

Burrows, D. 2000 Using GeoTIFF images to create flexible radar compositing software. *Phys. Chem. Earth Pt B* **25** (10–12), 1137–1140.

Ciach, G. J. 2003 Local random errors in tipping-bucket rain gauge measurements. *J. Atmos. Oceanic Technol.* **20**, 752–9.

Chumchean, S., Seed, A. & Sharma, A. 2008 An operational approach for classifying storms in real-time radar rainfall estimation. *J. Hydrol.* **363**, 1–17.

Crane, R. K. 1979 Automatic cell detection and tracking. *IEEE Trans. Geosci. Elect.* **GE-17**, 250–262.

Cremonini, R. & Bechini, R. 2010 Heavy rainfall monitoring by polarimetric C-Band weather radars. *Water* **2**, 838–848.

Crocker, J. C. & Grier, D. G. 1996 Methods of digital video microscopy for colloidal studies. *J. Colloid Interface Sci.* **179** (1), 298–310.

Daliakopoulos, I. N., Koutroulis, A. G. & Tsanis, I. K. 2006 Uncertainty assessment in historical precipitation time series. *Geophys. Res. Abstr.* **8**, 03034.

Delrieu, G., Braud, I., Berne, A., Borga, M., Boudevillain, B., Fabry, F., Freer, J., Gaume, E., Nakakita, E., Seed, A., Tabary, P. & Uijlenhoet, R. 2009 Weather radar and hydrology. *Adv. Water Res.* **32** (7), 969–974.

Divjak, M., Le Berre, P., Bižić, D., Ciotti, C., Rosa Dias, M., Galli, G., Huuskonen, A., Kotláriková, J., Nágy, J., Schreiber, K.-J. & Wheeler, W. K. 1999 Radar data quality-ensuring procedures at European weather radar stations. Eumetnet Opera Programme, Subproject 1c/1, OPERA/WD/9/1999.

Djurcilov, S. & Pang, A. 1999 Visualizing gridded datasets with large number of missing values (case study). In *Proceedings of the conference on Visualization '99: celebrating ten years table of contents*, San Francisco, United States, pp. 405–408.

Doviak, R. J. & Zrnić, D. S. 1993 *Doppler Radar and Weather Observations*. 2nd edition, Academic Press, San Diego.

Durden, S. L., Haddad, Z. S., Kitiyakara, A. & Li, F. K. 1998 Effects of nonuniform beam filling on rainfall retrieval for the TRMM precipitation radar. *J. Atmos. Oceanic Technol.* **15** (3), 635–646.

EEC 2011 *EDGE Radar Control and Data Analysis Software*. Available from: www.eecradar.com (accessed 9 September 2011).

Einfalt, T., Denoeux, T. & Jacquet, G. 1990 A radar rainfall forecasting method designed for hydrological purposes. *J. Hydrol.* **114** (3–4), 229–244.

ESRI 1992 *Understanding GIS: The ArcInfo Method*. ESRI Press, Redlands, CA.

Fabry, F., Bellon, A., Duncan, M. R. & Austin, G. L. 1994 High resolution rainfall measurements by radar for very small basins: the sampling problem reexamined. *J. Hydrol.* **161**, 415–28.

Farid, H. 2008 *Fundamentals of Image Processing*. Available from: http://www.cs.dartmouth.edu/farid/downloads/tutorials/fip.pdf (accessed 9 September 2011).

Gao, J., Brewster, K. & Xue, M. 2006 A comparison of the radar ray path equations and approximations for use in radar data assimilation. *Adv. Atmos. Sci.* **23** (2), 190–198.

Goovaerts, P. 1997 *Geostatistics for Natural Resources Evaluation*. Oxford University Press, New York, Oxford.

Harrold, T. W., English, E. J. & Nicholas, C. A. 1974 The accuracy of radar-derived rainfall measurements in hilly terrain. *Q. J. Roy. Meteor. Soc.* **100**, 331–350.

Jackson, M. E. 1993 An echo motion algorithm for air traffic management using a national radar mosaic. In *Preprints, Fifth International Conference on Aviation Weather Systems*, American Meteor Society, Vienna, VA, pp. 299–303.

Johnson, J. T., Mackeen, P. L., Witt, A., DeWayne Mitchell, E., Stumpf, G. J., Eilts, M. D. & Thomas, K. W. 1998 The storm cell identification and tracking algorithm: an enhanced WSR-88D algorithm. *Weather Forecast.* **13** (2), 263–276.

Joss, J. & Lee, R. 1995 The application of radar–gauge comparisons to operational precipitation profile corrections. *J. Applied Meteorol.* **34**, 2612–2630.

Joss, J. & Waldvogel, A. 1990 Precipitation measurement and hydrology. In: *Radar in Meteorology* (D. Atlas, ed.). American Meteorological Society, Boston, pp. 577–606.

Kitchen, M. & Jackson, P. M. 1993 Weather radar performance at long Range-Simulated and observed. *J. Applied Meteorol* **32**, 975–985.

Krajewski, W. F. & Ciach, G. J. 2004 Towards operational probabilistic quantitative precipitation estimation using weather radar. In *Sixth International Symposium on Hydrological Applications of Weather Radar*, Melbourne.

Kyznarová, H. & Novák, P. 2009 Rain pattern tracking by means of COTREC and modal matching. *Atmos. Res.* **93**, 317–327.

Lim, J. S. 1990 *Two-Dimensional Signal and Image Processing*. Prentice Hall, Englewood Cliffs, NJ, pp. 536–540.

Lindeberg, T. 1998 Edge detection and ridge detection with automatic scale selection. *Int. J. Computer Vision* **30** (2), 117–154.

Maybeck, P. S. 1979 *Stochastic Models, Estimation, and Control, Volume 1*. Academic Press, New York.

Mecklenburg, S., Jurczyk, A., Szturc, J. & Osrodska, K. 2002 *Quantitative Precipitation Forecasts (QPF) Based on Radar Data for Hydrological Models, COST Action 717: Use of Radar Observations in Hydrological and NWP Models*. Topic WG1–8. Available from: http://www.smhi.se/hfa_coord/cost717/doc/WDF_01_200203_2.pdf (accessed 9 September 2011).

Michelson, D., Einfalt, T., Holleman, I., Gjertsen, U., Friedrich, K., Haase, G., Lindskog, M. & Jurczyk, A. 2005 *Weather Radar Data Quality in Europe: Quality Control and Characterization*. Technical report, European Commission. COST 717 Final Document.

Naoum, S. & Tsanis, I. K. 2003 Hydroinformatics in evapotranspiration estimation. *Environ. Modell. Softw.* **18** (3), 261–271.

Naoum, S. & Tsanis, I. K. 2004 Orographic precipitation modelling with multiple linear regression. *J. Hydraul. Eng.* **9** (2), 79–102.

Nicol, J., Delrieu, G., Faure, D. & Tabary, P. 2004 Radar observation of intense rain events during the Bollene 2002 experiment. In *Sixth International Symposium on Hydrological Applications of Weather Radar*, Melbourne, Australia.

Paulitsch, H., Teschl, F. & Randeu, W. L. 2009 Dual-polarization C-band weather radar algorithms for rain rate estimation and hydrometeor classification in an alpine region. *Adv. Geosci.* **20**, 3–8.

Rosenfeld, D. 1987 Objective method for analysis and tracking of convective cells as seen by radar. *J. Atmos. Oceanic Technol.* **4**, 422–434.

Seminario, M., Gojara, K. & Chandrasekar, V. 2001 Noise correction of polarimetric radar measurements. In *Preprints, 30th International Conference on Radar Meteorology*, American Meteor Society, Munich, Germany, pp. 38–40.

Simonett, D. S. 1970 Remote Sensing with imaging radar: a review. *Geoforum* **1** (2), 61–74.

Simpson, T. W., Mauery, T. M., Korte, J. J. & Mistree, F. 1998 Comparison of response surface and Kriging models for multidisciplinary design optimization. 7th AIAA/USAF/NASA/ISSMO Symposium on Multidisciplinary Analysis & Optimization, St. Louis, MI, AIAA-98-4755.

Sugier, J., Parent du Châtelet, J., Roquain, P. & Smith, A. 2002 Detection and removal of clutter and anaprop in radar data using a statistical scheme based on echo fluctuation. In *Proceedings of ERAD*, pp. 17–24.

Teschl, R., Randeu, W. L. & Teschl, F. 2007 Improving weather radar estimates of rainfall using feed-forward neural networks. *Neural Networks* **20**, 519–527.

Tsanis, I. K. & Gad, M. A. 2001 A GIS precipitation method for analysis of storm kinematics. *Environ. Modell. Softw.* **16**, 273–281.

Tsanis, I. K., Gad, M. A. & Donaldson, N. T. 2002 A comparative analysis of rain-gauge and radar techniques for storm kinematics. *Adv. Wat. Res.* **25**, 305–316.

Toussaint, M., Jacquemin, B., Donet, I., Carlier, A. & Malkomes, M. 2000a GSF – a Doppler weather radar based tracking tool. *Phys. Chem Earth (B)* **25** (10–12), 1339–1342.

Toussaint, M., Malkomes, M., Hagen, M., Höller, H. & Meischner, P. 2000b A real time data visualization and analysis environment, scientific data management of large weather radar next term archives. *Phys. Chem Earth (B)* **25** (10–12), 1001–1003.

Uijlenhoet, R., van der Wielen, S. H. & Berne, A. 2006 Uncertainties in rainfall retrievals from ground-based weather radar: overview, case study, and simulation experiment. *Hydrol. Earth Syst. Sci. Discuss.* **3**, 2385–2436.

Villarini, G., Serinaldi, F. & Krajewski, W. 2008 Modeling radar-rainfall estimation uncertainties using parametric and non-parametric approaches. *Adv. Wat. Res.* **31**, 1674–1686.

Wiener, N. 1949 *Extrapolation, Interpolation, and Smoothing of Stationary Time Series*. Wiley, New York.

Wildenauer, H., Mičušík, B. & Vincze, M. 2007 *Efficient Texture Representation Using Multi-scale Regions. Chapter in Computer Vision – ACCV 2007*. Springer, Berlin/Heidelberg.

Wilk, K. E. & Gray, K. C. 1970 Processing and analysis techniques used with the NSSL weather radar system. In *Preprints, 14th Radar Meteorology Conference*, American Meteor Society, Tucson, AZ, pp. 369–374.

Wilson, J. W. & Brandes, E. A. 1979 Radar measurement of rainfall – A summary. *B. Am. Meteorol. Soc.* **60**, 1048–1058.

Zawadzki, I. 1984 Factors affecting the precision of radar measurements of rain. In *Preprints of Conference of Radar Meteorology*, AMS, Zurich, pp. 251–256.

Zittel, W. D. 1976 Computer applications and techniques for storm tracking and warning. In *Preprints, 17th Conference on Radar Meteorology*, American Meteorological Society Seattle, WA, **60**, pp. 514–521.

Ziyang, M., Xiaoyu, H., Lizhi, C. & Wendong, H. 2008 *Weather Radar Image Filtering with Fuzzy Features Using Non Linear Technique*. Congress on Image and Signal Processing. CISP '08. 2, pp. 201–205. China, ISBN:978-0-7695-3119-9.

First received 9 September 2010; accepted in revised form 23 March 2011. Available online 14 July 2011